Technical Report

TR-03-04

Study of the role of magnetite in the immobilisation of U(VI) by reduction to U(IV) under the presence of H_2(g) in hydrogen carbonate medium

Miquel Rovira, Joan de Pablo
Centre Tecnològic de Manresa, Spain

Souad El Aamrani
Universitat Politècnica de Catalunya, Spain

Lara Duro, Mireia Grivé, Jordi Bruno
Enviros Spain SL, Spain

January 2003

Svensk Kärnbränslehantering AB
Swedish Nuclear Fuel
and Waste Management Co
Box 5864
SE-102 40 Stockholm Sweden
Tel 08-459 84 00
+46 8 459 84 00
Fax 08-661 57 19
+46 8 661 57 19

Study of the role of magnetite in the immobilisation of U(VI) by reduction to U(IV) under the presence of H_2(g) in hydrogen carbonate medium

Miquel Rovira, Joan de Pablo
Centre Tecnològic de Manresa, Spain

Souad El Aamrani
Universitat Politècnica de Catalunya, Spain

Lara Duro, Mireia Grivé, Jordi Bruno
Enviros Spain SL, Spain

January 2003

Abstract

This report corresponds to the work carried out during the period March 2001–July 2002. The interaction of Uranium(VI) in hydrogen carbonate medium with commercial magnetite as well as with magnetite formed as a corrosion product on the surface of a steel coupon has been studied. The influence of the hydrogen pressure and the mass of magnetite have been two of the factors studied in detail.

Results obtained with commercial magnetite indicates that uranium concentration in solution can be explained taking into account the solubility of UO_2(am) at the experimental conditions employed (pe+pH≈6) and at different hydrogen pressures. The uranium(VI) reduction has been clearly demonstrated by using X-Ray Absorption Near Edge Structure (XANES). Experiments performed during 30 days in hydrogen atmosphere showed a reduction of the 80% of U(VI). Results obtained by using X-Ray Photoelectron Spectroscopy also corroborate the U(VI) reduction on the surface of the magnetite.

In the case of magnetite obtained on a steel coupon, it seems that the presence of zero-valent iron below the magnetite surface might account for an increase of the electronic density at the surface and, therefore causing a preferential oxidation of the structural iron in front of the experiment conducted with commercial magnetite. Uranium concentration seems also to be controlled by UO_2(am) solubility.

Contents

1 Introduction

Under anoxic conditions, Fe corrodes, in a first step, to produce $Fe(OH)_2(s)$, which, in turn can experiment the Schikorr reaction to transform into magnetite, Fe_3O_4:

$$Fe(s) + 4\ H_2O = Fe_3O_4(s) + 4\ H_2$$

Although the intermediate product of the anoxic corrosion of steel depends on the conditions of the corrosion media, i.e. under carbonate solutions $FeCO_3(s)$ are more likely to form than $Fe(OH)_2$, it seems clear that the final anoxic corrosion product is a magnetite-type spinel. For this reason, the study of the role of magnetite in retaining radionuclides is an issue of crucial importance for the performance assessment of a nuclear spent fuel repository. The semiconductor character of this solid points out its potential redox capacity in the system and leads us to consider its role as mediator in the reduction of actinides which result in an immobilisation of these elements via precipitation of the more insoluble Actinide(IV) solid phases.

Previous works in the literature /White and Peterson, 1996/ conducted at the acidic pH region observed that magnetite and ilmenite had important reduction effects on Cr(VI), Cu(II), V(V) and Fe(III). In the present work we document the results obtained from the study of the role of $Fe_3O_4(s)$ in mediating the reduction of U(VI) to U(IV).

It seems clear that both, homogeneous and heterogeneous reduction of U(VI) by the structural iron of magnetite or by the ferrous iron released from its dissolution process are likely to occur under the investigated conditions.

The analyses of the iron concentration in solution and its redox speciation is of the utmost importance to obtain a clearer picture of the observed phenomena.

The present work highlights the relevance of the reductive capacity of the spent fuel/iron inlet system in defining the release behaviour of actinides from the waste matrix. The work already in progress gives quantitative information on the mechanisms and extent of this reductive capacity.

One of the drawbacks we had during the previous stage was the control of the pH of the system. In that case the pH evolved due to the evolution of CO_2 by the continuous $H_2(g)$ bubbling forced through the solutions. This produced an increase in pH as it was already demonstrated by geochemical calculations /Parkhurst and Appelo, 1999/ (see Figure 1).

Given this lack of control of one of the master variables of our system we decided to keep constant the $CO_2(g)$ partial pressure in the system and use a mixture of $H_2(g) + CO_2(g)$ with a $\log pCO_2(g) = -3.82$, slightly lower than the atmospheric value.

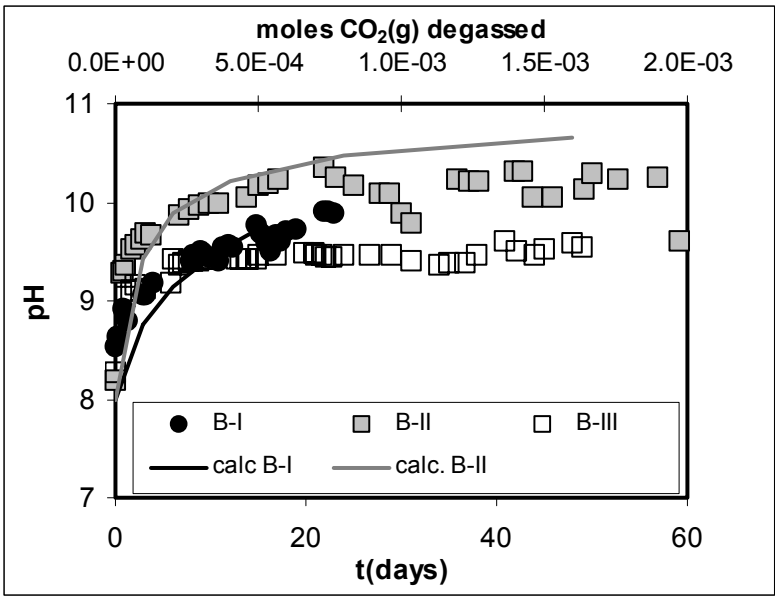

Figure 1. *Evolution of the pH in solution in Tests B, conducted at 1 atm H_2(g), 2 g of magnetite per 0.2 dm^3 of ionic medium with an initial carbonate concentration of $2 \cdot 10^{-3}$ M (B-I) and $5 \cdot 10^{-4}$ M (B-II). The experiment B-III contained a lower weight of magnetite (0.1 g) in the same solution volume and an initial carbonate concentration of $5 \cdot 10^{-4}$ M.*

2 Experimental methodology

2.1 Experimental program

There are some points that deserve an special attention in the system we are studying. Given that the main uncertainty is associated to which is the actual process accounting for the decrease in the uranium concentration in the solution, and how the master variables of the system respond to this decrease we set up the following experimental program.

Tests conducted at a P = 1 atm

Test Cont. III. This experiment was already conducted in the last stage of the project, but no proper iron analyses was conducted due to analytical limitations. We have studied the behaviour of commercial magnetite under the presence of $P(H_2) = 1$ atm. A given volume of ionic media has been put in contact with a given weight of crushed magnetite. A continuous $H_2(g)+CO_2(g)$ bubbling has been kept through the system, which allows a control on the carbonate system. We have monitored the evolution of the solution and of the surface of the solid with time by means of XPS.

Tests Redox. Study of the response of the redox electrode to the iron or the uranium systems. We have tested the response of two redox electrodes (Pt and Au) to the Fe(II)/Fe(III) and U(VI)/U(IV) systems under $P(H_2) = 1$ atm. To this regard the dependence of the measured redox potential with the concentration of these two redox pairs has been investigated.

Tests B and N. Study of the effect of commercial magnetite on the behaviour of U(VI) under the presence of $p(N_2(g))+p(CO_2(g)) = 1$ atm (N) or $p(H_2(g))+ p(CO_2(g)) = 1$ atm (B). A given volume of ionic media has been spiked with a solution of uranium(VI) under a continuous $H_2(g)$ bubbling; a weighed amount of crushed and sieved magnetite has been then added to the experiment. These experiments may allow us to assess whether the reduction process is also observed under anoxic conditions.

Tests D and FE

D-II: Study of the effect of the magnetite formed on the surface of an steel coupon on the behaviour of U(VI) under the presence of $p(H_2(g))+ p(CO_2(g)) = 1$ atm.

FE: Study of the effect of an steel coupon on the behaviour of U(VI) under the presence of $p(H_2(g))+ p(CO_2(g)) = 1$ atm.

The aim of these tests is to ascertain whether the presence of steel in the system affects to an important extent to the reduction process.

Tests conducted at a P > 1 atm

In order to test the influence of a hydrogen overpressure on the system under study, several tests have been conducted at different $P(H_2(g))$ (tests C) contacting weighted amounts of magnetite with uranium solutions, and following uranium concentrations as a function of time. Samples of the solution have been withdrawn for uranium analyses. The experimental design considers a very tight control of the uranium concentration during the first 24 h of the experiment in order to assess the relevance of the hydrogen overpressure on the rate of reduction of uranium.

The matrix of experimental conditions is shown in Table 1.

Table 1. Experimental conditions. All experiments conducted with an ionic medium of 0.01 M NaCl. Shadowed rows indicate the experiments conducted at this 2nd. stage of the project, while "1" in the STAGE column indicates experiments conducted during the previous stage.

Test	STAGE	$Fe_3O_4(s)$ (g)	$[U(VI)]_o$ (mol dm^{-3})	$[NaHCO_3]_o$ (mol dm^{-3})	$P(N_2)$ (atm)	Initial and Final $P(H_2)$ (atm)
Cont. I	1	2	–	$5\cdot10^{-4}$	–	1
Cont. II	1	–	$1.0\cdot10^{-5}$	$2\cdot10^{-3}$	–	1
Cont. III	2	2		–3.82*	–	1
B-I	1	2	$8.9\cdot10^{-6}$	$2\cdot10^{-3}$	–	1
B-II	1	2	$8.4\cdot10^{-6}$	$5\cdot10^{-4}$	–	1
B- III	1	0.1	$8.1\cdot10^{-6}$	$5\cdot10^{-4}$	–	1
B-IV	2	2		–3.82*	–	1
N-I	2	2		–3.82*	1	–
B-V	2	20		–3.82*		1
C-IV	2	2	$7.3\cdot10^{-6}$	$5\cdot10^{-4}$		2.2–1.3
C-I	1	2	$1.1\cdot10^{-5}$	$5\cdot10^{-4}$		4.1–3.4
C-II	1	2	$8.3\cdot10^{-6}$	$5\cdot10^{-4}$		7.5–6.6
C-III	1	0.1	$7.3\cdot10^{-6}$	$5\cdot10^{-4}$		7.5–5.5
C-V	2	5	$7.5\cdot10^{-6}$	$5\cdot10^{-4}$		8.6–4.0
D-I	1	CC	$8.1\cdot10^{-6}$	$5\cdot10^{-4}$		1
D-II	2	CC		–3.82*		1
FE	2	FC		–3.82*		1

CC: Corroded carbon steel coupon

FC: Fresh carbon steel coupon

* log $pCO_2(g)$ kept constant

Tests for XAS analyses

Given the lack of clear conclusions obtained during the previous stage of the project concerning the effective reduction of uranium onto the surface of the solid magnetite we have conducted several XAS analyses at the Rossendorf Operating BeamLine at the European Research Synchroton Facility of Grenoble. In order to have proper data from this technique we have prepared different samples by maximising the solid-solution contact with a methodology of recirculation of the solution through the solid. The samples were prepared both under nitrogen and under hydrogen atmosphere with the aim of identifying differences in the results. The presentation of the results obtained by this technique and the scientific basis for their analyses are presented in a separated section of this report.

2.2 Materials

2.2.1 Solid phases

The magnetite used in this work was supplied by Aldrich, with a purity of 98%, particle size less than 5 μm and surface area equal to 1.58 ± 0.01 m^2 g^{-1}. The X-Ray diffractogram showed a small percentage of Iron(III) oxide /El Aamrani et al, 1999/.

2.2.2 Chemicals

Chemicals used in this work, $UO_2(NO_3)_2.6H_2O$, $FeCl_2.4H_2O$, $FeCl_3.6H_2O$ NaCl(s) and $NaHCO_3$(s) were of analytical grade and supplied by Merck. All solutions were prepared with bidistilled water from a Millipore Corp. Milli-Q system.

2.3 Experimental procedures

In all the experiments 200 cm^3 of test solution were put in contact with weighed amounts of magnetite (see Table 1). Once the solid phases were introduced into the reactors, aqueous samples (1 cm^3) were taken periodically allowing uranium and iron analysis. Samples were immediately filtered through a 0.22 μm pore size filter and acidified by adding a small volume of concentrated HNO_3.

All the experiments were performed at room temperature. Two different reactors were employed depending on the H_2 overpressure under which the tests were carried out. Careful and continuous stirring of the reactors was ensured by means of an orbital agitator.

The pH of the solutions was monitored by means of a calibrated combined-glass electrode. Redox potentials were measured with a platinum electrode and the measurements were against the Ag/AgCl(s) and KCl saturated reference of the combined glass electrode. In the case of Redox Tests, an additional gold electrode was introduced in the reactor in order to compare redox potential values obtained with platinum and gold electrodes.

a) Tests conducted at a $P(H_2) = 1$ atm

The experiments were performed in the batch reactor shown in Figure 2. Tests solutions were continuously purged with $H_2(g)$ containing 0.015 atm of $CO_2(g)$. The gas stream was initially flushed through a solution of Cr(II) in contact with a Zn/Hg amalgam in order to avoid the introduction of oxidants into the system.

During the course of the experiments pH and pe were continuously monitored.

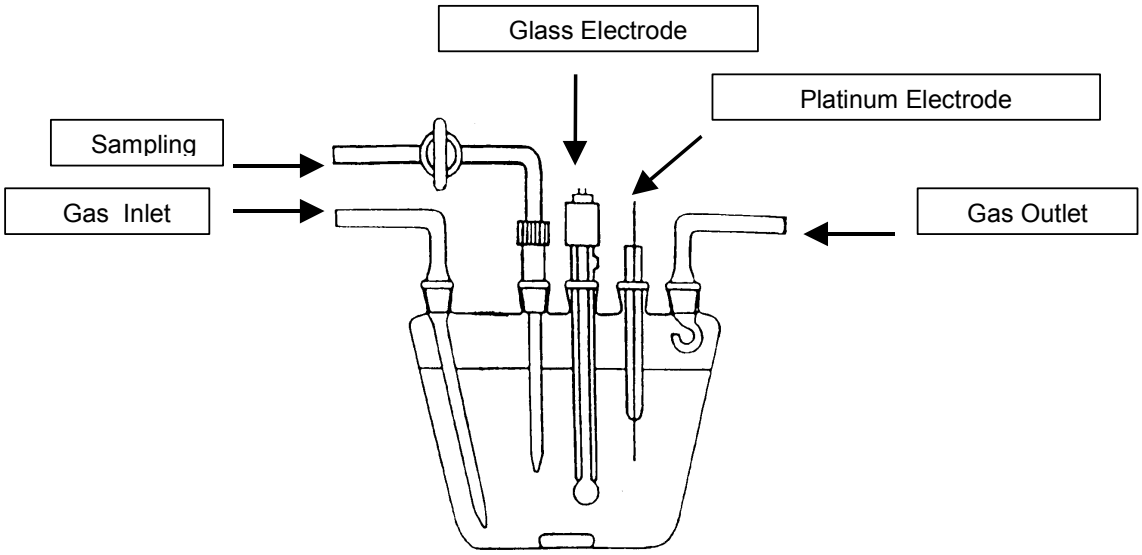

Figure 2. *Reactor employed in the experiments performed at $P(H_2) = 1$ atm.*

b) Tests conducted at a $P(H_2) > 1$ atm

The experiments were carried out in the steel autoclave depicted in Figure 3. In this case, continuous bubbling of $H_2(g)$ through the reactor was not possible. Thus, before the start of the experiment, the test solution was deaerated by bubbling H_2 during 2 hours. Afterwards, the solution and the corresponding solid phase were contacted and immediately transferred into the steel autoclave, which was brought up to its operating pressure by means of a routine avoiding the inlet of O_2 into the reactor.

pH measurements in the aqueous solutions were performed before and after the experiments.

During the tests H_2 overpressure diminished due to withdrawal of liquid samples from the reactor. For instance, sampling $1cm^3$ of liquid phase lead to a slight decrease of the H_2 overpressure: 0.1–0.2 atm. Considering the numerous samples withdrawn, significant H_2 overpressure variation occurred during the tests as can be seen in Table 1.

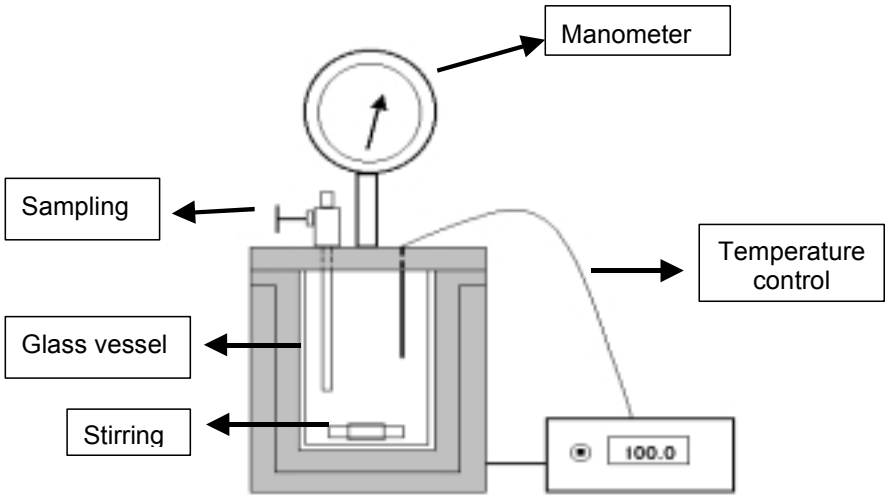

Figure 3. Autoclave steel reactor employed in the experiments performed at $P(H_2) > 1$ atm.

c) Anaerobic corrosion of carbon steel

The surface of a carbon steel coupon having dimensions of 30 x 30 x 1 mm was cleaned by pickling in 10% HCl, followed by thorough washing in distilled water and absolute alcohol in order to remove the air-form oxide film. Subsequently, the coupon was immersed in a solution (150 cm^3) having the composition: $5 \cdot 10^{-4}$ mole dm^{-3} $NaHCO_3$ and 0.02 mol dm^{-3} NaCl and previously deaerated with H_2 during 2 hours. Thereafter, the coupon and the solution were transferred to the steel autoclave (Figure 3) which was brought to the optimum operating conditions for anaerobic corrosion of carbon steel: $P(H_2)$ = 8.4 atm and T = 90ºC /Blackwood et al, 1995/. The time span for reaching the operating temperature was less than 1 hour and the coupon was exposed to the corrosive environment for 20 days.

d) Redox tests

Redox tests were conducted in absence of magnetite with the aim to study the response of the redox potential to the iron and uranium systems. The experiments were performed using the batch reactor depicted in Figure 2 with permanent H_2 (nominally pure, 99.999%) bubbling and continuous pH and pe (gold and platinum electrodes) monitoring.

For the Iron-Uranium Redox Test (IURT), the experiment has been divided in several parts depending on the experimental conditions employed as can be seen in Table 2. In the case of Uranium Redox Tests (URT), the evolution of a solution $2 \cdot 10^{-3}$ $moldm^{-3}$ of U(VI) at initial pH 2.3 (adjusted with $HClO_4$) in the presence of a palladium black catalyst, was followed as a function of time.

Table 2. Experimental conditions used in Iron Uranium Redox Tests (IURT).

	Time (days)	Conditions	pH
Part A	0	10^{-3} mol dm^{-3} Fe(II) and 10^{-5} mol dm^{-3} Fe(III)	2.1
	30		2.1
Part B	30	Pulse of $8.7 \cdot 10^{-5}$ mole Fe(III) into174 ml	2.1
	85		1.9
Part C	85	Introduction of a palladium black catalyst	1.9
	96	(platinum electrode removed)	1.9
Part D	96	Pulse of $1.6 \cdot 10^{-4}$ mole U(VI) into158 ml	1.9
	99		1.9

2.4 Solution analysis

Uranium concentrations in the aqueous solutions were determined using an ICP-MS (Inductively Coupled Plasma Mass Spectrometer) Perkin Elmer Elan 6000.

Ferric ion was indirectly determined by first reducing total Fe with hydroxilamine and subtracting out the previously measured ferrous concentration. Iron(II) concentration was analysed spectrophotometrically in aqueous solution as the iron(II) complex with the disodium salt of ferrozine. Total iron concentration was determined previous reduction of iron (III) to iron(II) using the same analytical method. /Gibbs, 1976/.

2.5 Surface analysis

Magnetite was examined by X-Ray Photoelectron Spectroscopy (XPS) before and after exposure to the test solution in the Test Control 1 allowing semi-quantitative analysis of the magnetite surface composition. Spectra were recorded on a PHI Perkin Elmer ESCA Multianalyzer 5500. Uranium analysis on the magnetite surface by XPS was performed with the same apparatus for sample from Test C-V.

The carbon steel coupon exposed to the corrosive environment, once was removed from the autoclave was examined by X-Ray Diffraction (XRD) in order to identify the corrosion products generated on its surface. XRD spectra were obtained using a Bruker D-5005 instrument.

3 Experimental results and discussion

3.1 Behaviour of magnetite at $pH_2(g)$ = 1 atm

Information on the chemical composition of magnetite surface in this test (Test control I) was obtained using XPS. /McIntyre and Zetaruk, 1977/ achieved proper discrimination of the ferrous and ferric components in the XPS Fe(3p) spectrum. They deconvoluted the Fe(3p) signal in three different peaks allowing to determine the relative concentration of Fe(II) and Fe(III) on the magnetite surface. The lower binding energy peak represents the Fe(II) contribution while the two peaks at high binding energy reflect the Fe(III) contribution.

The spectra corresponding to the surfaces of both untreated magnetite and the magnetite after the completion of the test are illustrated in Figures 4 and 5. The previously described procedure has been applied to the analysis of magnetite surfaces, and the deconvolution of the Fe(3p) peaks are also shown in Figures 4 and 5. The obtained Fe(II)/Fe(III) ratios are listed in Table 3.

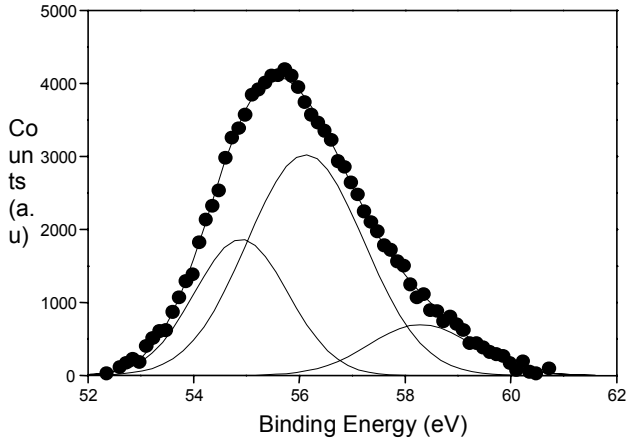

Figure 4. *Fe(3p) spectra of unreacted magnetite.*

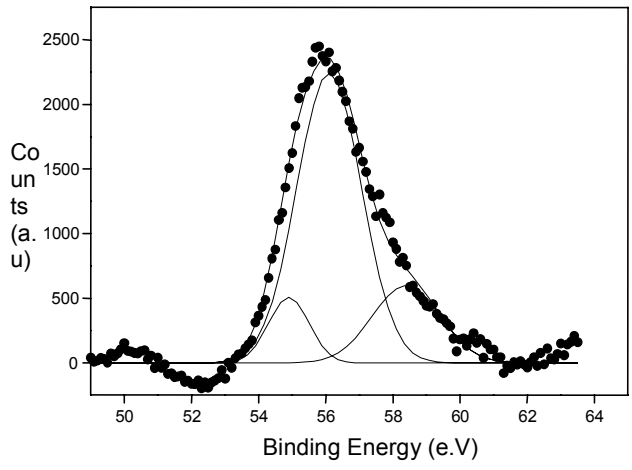

Figure 5. *Fe(3p) spectra of magnetite after Test Control 1.*

Table 3. Fe(II)/Fe(III) ratios of magnetite surfaces.

Sample	Fe(II)/Fe(III) Ratio
Unreacted magnetite	0.5
Magnetite after Test Control I	0.1
Magnetite after Test Control III	0.5

From the data in Table 3, it can be noticed that for unreacted magnetite the Fe(II)/Fe(III) ratio is 0.5, which is in excellent agreement with the theoretical ferrous/ferric stoichiometry of 0.5 in pure magnetite. On the other hand, the results obtained during the previous stage from Test Control I indicated that the surface of the solid underwent an increase in iron oxidation state during its dissolution, probably due to a preferential release of Fe(II) to the solution. As already mentioned, this was found to be in agreement with the observations reported by /White et al, 1994/, who studied the behaviour of magnetite electrodes and determined that the alteration of the solid could be expressed in terms of the following reaction:

$[Fe^{2+}Fe_2^{3+}]O_4$ (magnetite) + 2 H^+ = $[Fe_2^{3+}]O_3$ (maghemite) + Fe^{2+} + H_2O

Nevertheless when analysing the results obtained at this stage, i.e. the ones from Test Control III we observe that the oxidation state of iron at the surface is kept roughly constant. The only differences in the experimental setup between Test Control I and Test Control III is that in this later case the pH of the solution is constant. We saw in the previous stage of the project that the degassification of CO_2 from the solutions produced an increase in the pH of the medium what produced an stabilisation of Fe(III) with respect to Fe(II), i.e, the increase in pH favoured the oxidation (see Figure 6).

In Test Control III, though, pH is not varying and, therefore the carbonate content is kept constant. This was observed in previous experiments /El Aamrani et al, 1999/ when working with magnetite and carbonate in solution without any gas bubbling through the system that could force the CO_2 degassing process.

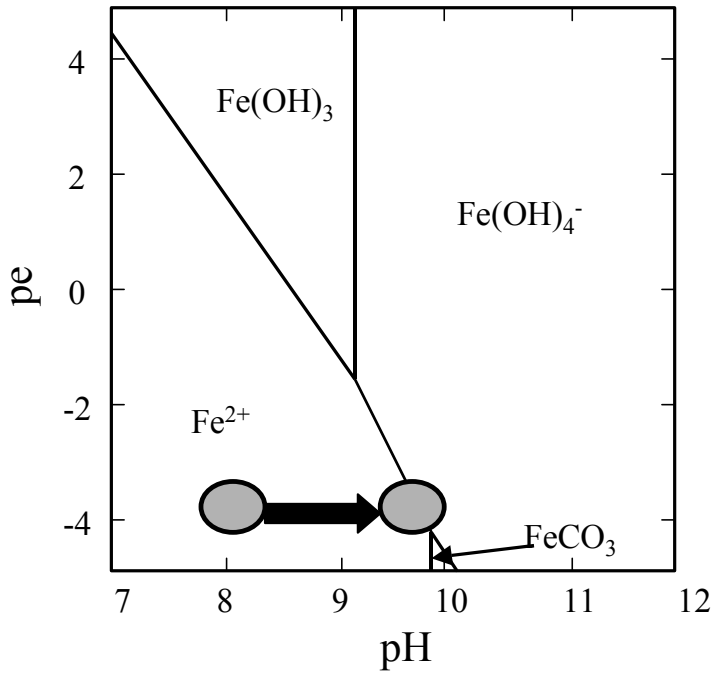

Figure 6. *Effect of an increase in pH in the system by assuming that the redox potential is kept constant.*

3.2 Redox control

Iron-Uranium Redox Test (IURT)

IURT has been divided in four parts (A, B, C and D) depending on the experimental conditions employed (see Table 2).

The initial solution containing 10^{-3} mol dm^{-3} Fe(II) and 10^{-5} mol dm^{-3} Fe(III) at pH 2.3 evolved towards the chemical equilibrium between Fe(II) and Fe(III) (see Equation (1)). Iron analysis in solution showed that Fe(III) concentration increased accompanied of a pe increase (see Figures 7 and 8), corresponding to an increase of the ratio $[Fe^{+3}]/[Fe^{+2}]$ in solution.

$$Fe^{+3} + e^{-} \Leftrightarrow Fe^{+2} \quad (1)$$

In Part B, after the addition of a Fe(III) pulse, the system was disturbed and a pe increase was forced, reaching a steady state. The experimentally measured pe values are in accordance with the theoretical calculated redox potential using Equation (2) and the measured Fe(II) and Fe(III) concentrations.

$$pe = pe_o + \log [Fe^{3+}]/[Fe^{2+}] \quad (2)$$

In Part C, the platinum electrode was substituted by a black palladium catalyst, and the response of the system was a rapid pe diminution coupled with a Fe(III) decrease in solution (Fe(II) increase) which confirms the previous observations. The decrease in pe in this case is likely to be a response of the system to the decrease of the ferric iron due to the catalytic effect of black palladium on the Fe(III) reduction by H_2 (see Equation (3)).

$$2\ Fe^{3+} + H_2 \Leftrightarrow 2\ Fe^{2+} + 2\ H^+ \qquad (3)$$

Finally, in Part D, an oxidant addition to the solution (U(VI)) induces a sudden redox potential increase followed by a subsequent pe diminution as a function of time, which may be explained in terms of disappearance of U(VI) by reduction and precipitation.

The experimentally measured pe both with Pt and Au electrodes is shown in Figure 7. From this figure we can see that both electrodes behave similarly and that Pt seems to give a slower response to the system.

From this experiment, we have concluded that the electrode response seems to be related to the oxidation state of the uranium and iron species in solution, and that both redox electrodes, gold and platinum, behave similarly.

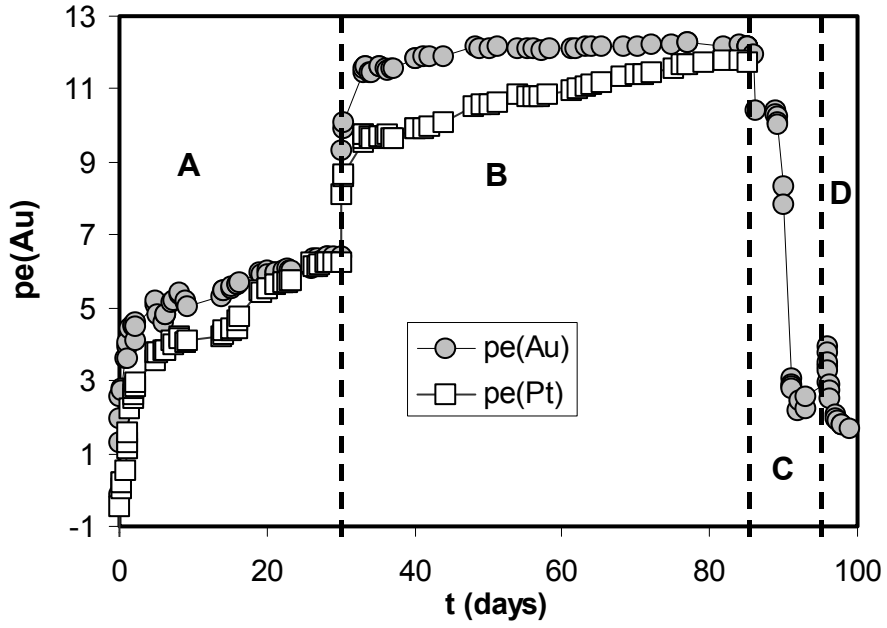

Figure 7*. Redox potential evolution (as a function of time in Iron-Uranium Redox Test (IURT)).*

Uranium Redox Test (URT)

In Figure 8 we present the evolution of uranium concentration and the redox potential with time of a solution initially having a concentration of 10^{-3} mol dm^{-3} U(VI) at pH 2.3 under continuous H_2 bubbling and the presence of a black palladium catalyst. In the first stage of the experiment (0 to 5 days) the uranium concentration and the pe decrease as a function of time, and a colour solution change was observed: yellow (U(VI)) to green (U(IV)). This process was also qualitatively followed by reading the U(VI) and U(IV) peaks absorbance at 414 nm and 648 nm respectively, using a UV-VIS spectrophotometer. The redox potential decreases, as if it were responding to an increase of reducing species in the system (see Equation (4)). After 5 days, the uranium concentration continued its decrease, however the redox potential was found to increase accompanied with the appearance of a black precipitate in the system, likely to be UO_2(s) (see Equation (4)). In this case, this pattern might be attributed to the removal of U(IV) species from the solution. The observed experimental trends, as in the case of IURT, highlight the fact that the redox electrode response seems to be related to the ratio oxidizing/reducing species in solution of the redox pairs involved in the system.

$$UO_2^{2+} + H_2 \Leftrightarrow UO_2\,(s) + 2\,H+ \qquad (4)$$

The final measured uranium concentration in the experiment is in agreement with the calculated solubility of UO_2(am) (log K_{s0} = 1.5, /Neck and Kim, 2001/) at the experimental conditions under which this experiment was performed.

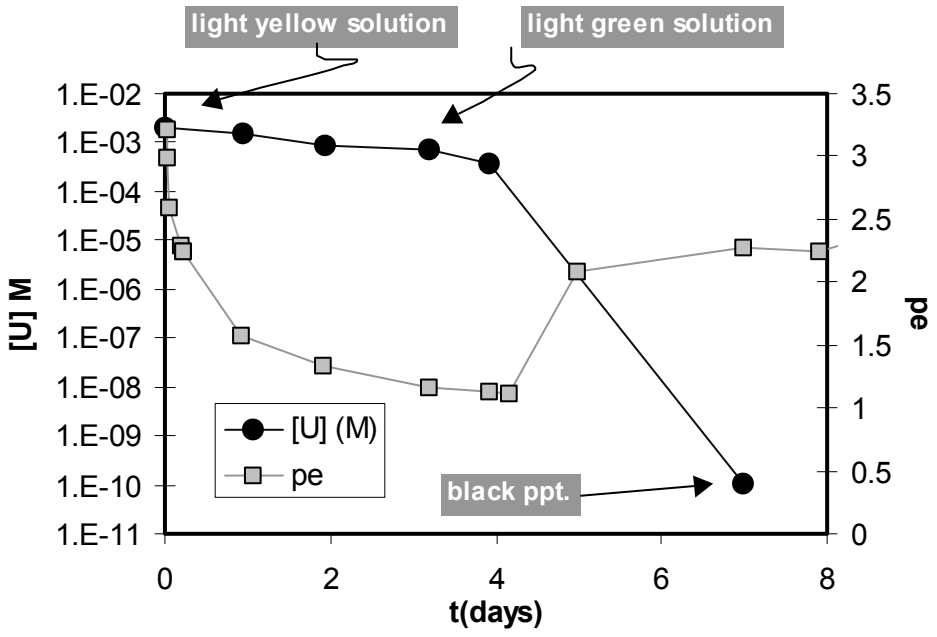

Figure 8. *Uranium concentration and measured pe as a function of time in Uranium Redox Test (URT).*

3.3 Effect of magnetite on the behaviour of U(VI) at $P(H_2)$ = 1 atm and $P(N_2)$ = 1 atm

Different experiments were conducted in an attempt to study the influence of the presence of magnetite on the behaviour of U(VI) at 1 atm pH_2.

In these experiments, during the previous stage of the project we investigated both, the effect of the carbonate concentration in solution (exp. B-I and B-II) and the effect of the mass of magnetite in the system (exp. B-II and B-III). At this new stage, we have studied the same system by keeping constant the pH via a continuous $H_2(g)$+$CO_2(g)$ bubbling through the solution (B-IV and B-V). Additionally a parallel experiment under anoxic conditions (N-I) has been conducted where a continuous bubbling of a mixture $N_2(g)$+ $CO_2(g)$, where log pCO_2 = –3.82 has been kept constant. A summary of the experimental conditions is shown in Table 4.

Table 4. Summary of the experimental conditions used in Tests B at 1 atm $H_2(g)$.

Test	Solid (g)	[U]o (mole/dm^3)	[$NaHCO_3$]o (mole/dm^3)	[NaCl] (mole/dm^3)
B-I	2	$8.9\cdot10^{-6}$	$2\cdot10^{-3}$	10^{-2}
B-II	2	$8.4\cdot10^{-6}$	$5\cdot10^{-4}$	10^{-2}
B-III	0.1	$8.1\cdot10^{-6}$	$5\cdot10^{-4}$	10^{-2}
B-IV	2	$8.1\cdot10^{-6}$	logpCO_2 = –3.82	10^{-2}
B-V	20	$8.1\cdot10^{-6}$	logpCO_2 = –3.82	10^{-2}
N-I	2	$1.05\cdot10^{-5}$	logpCO_2 = –3.82	10^{-2}

The evolution of the concentration of uranium in solution with time for these experiments is shown in Figure 9.

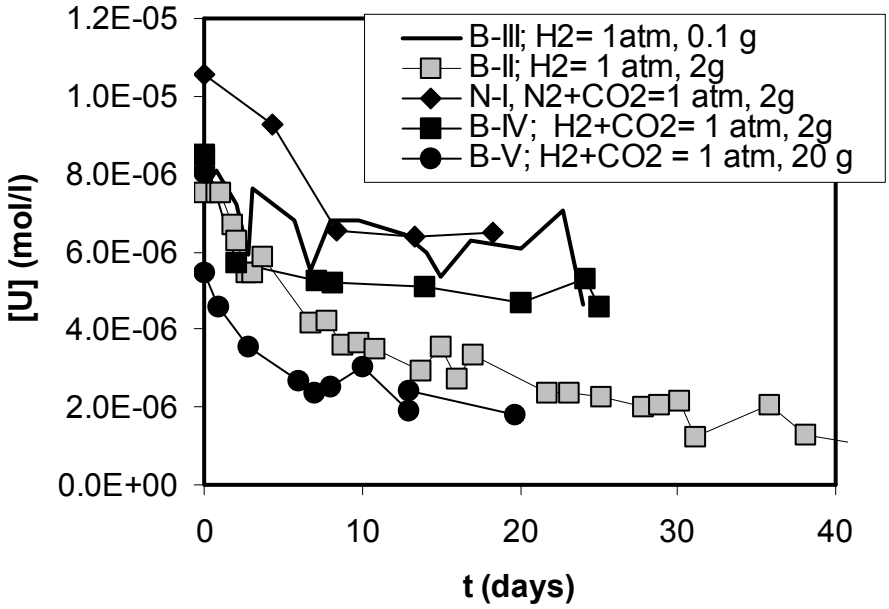

Figure 9. *Evolution of the concentration of uranium in solution in Tests at 1 atm.*

When comparing the final uranium concentrations obtained for experiments conducted under initial similar conditions, such as B-II and B-IV, we can see that in the case of B-II, the final concentration of uranium is lower. This is a consequence of the increase in pH observed in experiment B-II caused by the degassification of CO_2(g) driven by the H_2(g) bubbling. Therefore, the final concentration of carbonate in experiment B-II is lower than in experiment B-IV, where a stabilisation of the uranyl-carbonato complexes difficulties its reduction to U(IV) (see Figures 10 and 11).

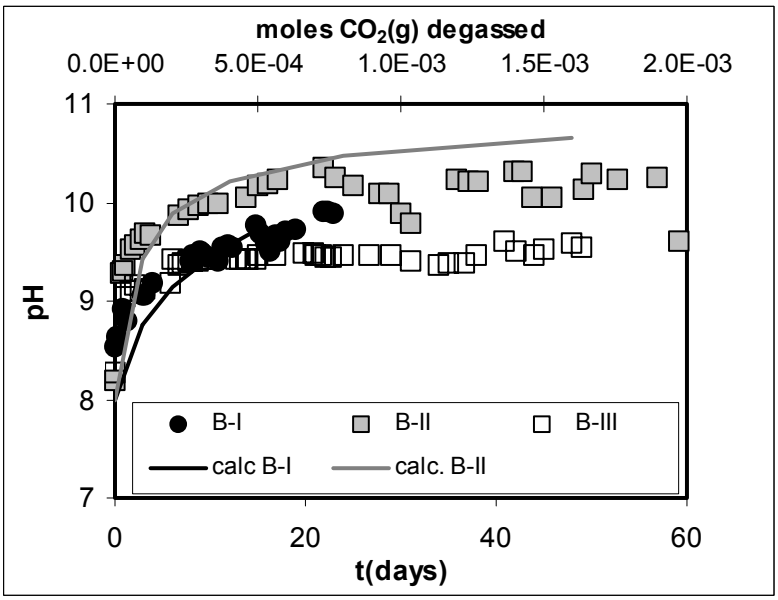

Figure 10. *Evolution of the pH in solution in Tests B conducted without CO_2(g) in the bubbling gas mixture.*

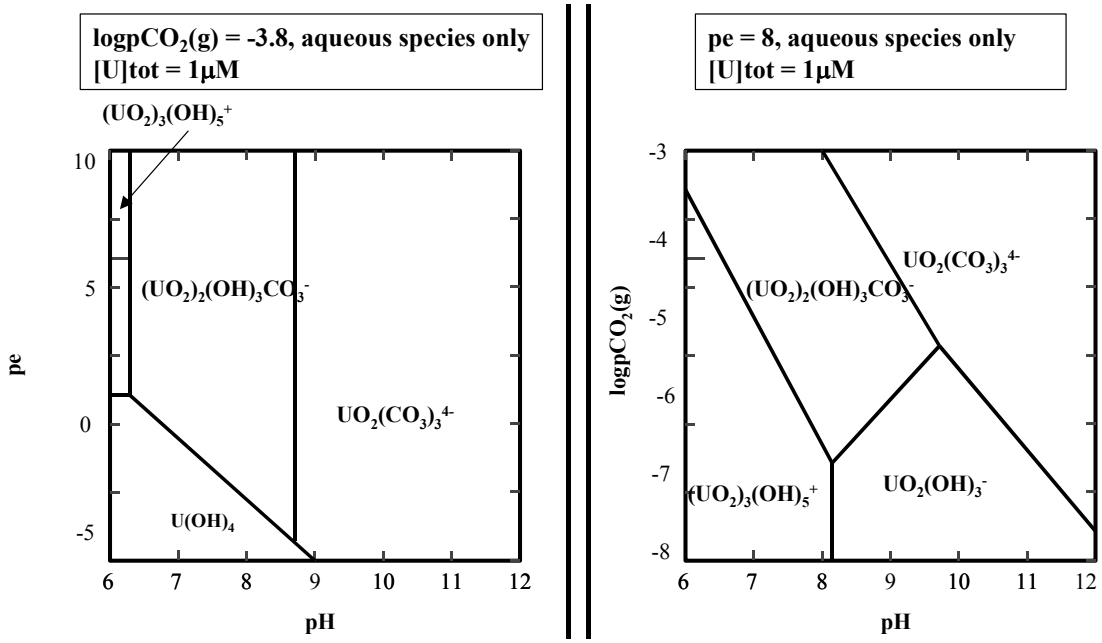

Figure 11. *Predominance diagram of the aqueous uranium system showing the influence of pe, pH and CO_2(g) partial pressure in the system.*

The stabilisation of the pH obtained in the tests conducted at this stage of the project can be compared with the previous experiments in Figure 12.

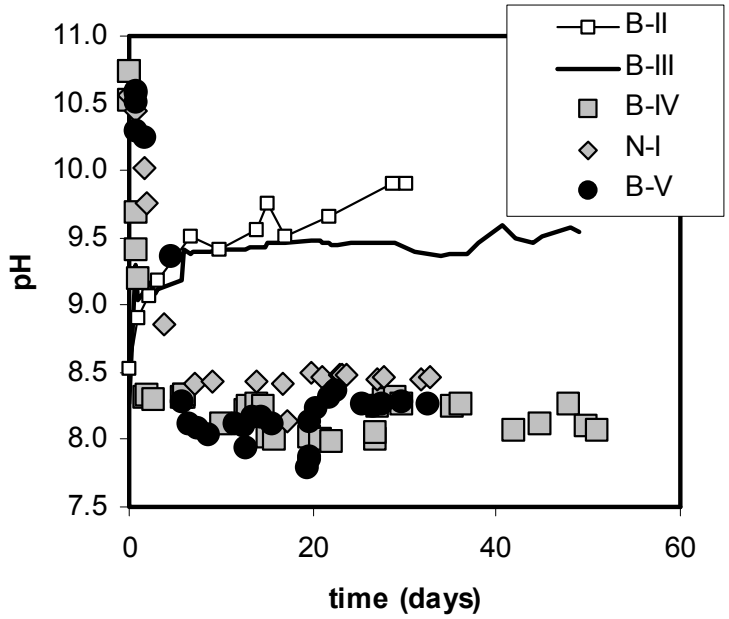

Figure 12. *pH evolution in the experiments. Increase of pH in B-II and B-III is caused by the degassification of CO_2(g) driven by the hydrogen bubbling.*

We can analyse how the final concentrations of uranium in each experiment can be explained as a steady state or as a thermodynamic equilibrium.

If uranium has undergone a reduction due to the presence of magnetite, the most likely solid to be precipitating is $UO_2(s)$, according to the following reaction in agreement with the speciation shown in Figure 11:

$$(UO_2)_2CO_3(OH)_3^- + 5\ H^+ + 4\ e^- = 2\ UO_2(s) + CO_2(g) + 4\ H_2O;\ \text{with log K} = 40.29 \quad (5)$$

In Figure 13 we can see the comparison between the solubility of $UO_2(am)$ calculated at $\log pCO_2(g) = -3.8$, i.e. the same conditions than the experiments at two different pe values: –2 and –3, which correspond to the range of values measured for these experiments. From this figure we can see that the measured uranium concentrations agree with the solubility of $UO_2(am)$ and, therefore that we may assume that a reduction process is occurring in the system.

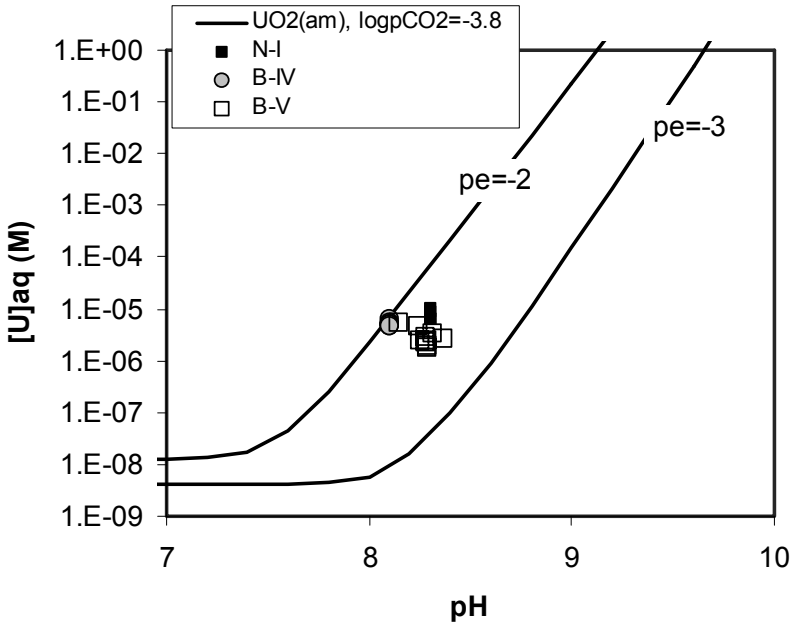

Figure 13. *Comparison between the solubility of $UO_2(am)$ and the experimental uranium concentrations measured in experiments N-I, B-IV and B-V.*

3.4 Effect of magnetite on the behaviour of U(VI) at $P(H_2) > 1$ atm

Different experiments were conducted at higher hydrogen overpressures. A summary of the experimental conditions is shown in Table 5.

Table 5. Summary of the experimental conditions of the tests performed at $p(H_2) > 1$ atm.

Test	Solid (g)	[U]o (mole/dm^3)	[$NaHCO_3$]o (mole/dm^3)	[NaCl] (mole/dm^3)
C-IV	2	$7.3 \cdot 10^{-6}$	$5 \cdot 10^{-4}$	2.2–1.3
C-I	2	$1.1 \cdot 10^{-5}$	$5 \cdot 10^{-4}$	4.1–3.4
C-II	2	$8.3 \cdot 10^{-6}$	$5 \cdot 10^{-4}$	7.5–6.6
C-III	0.1	$7.3 \cdot 10^{-6}$	$5 \cdot 10^{-4}$	7.5–5.5
C-V	5	$7.5 \cdot 10^{-6}$	$5 \cdot 10^{-4}$	8.6–4.0

Due to the experimental set up used in the tests conducted at $p(H_2) > 1$ atm, no monitoring of pH or pe was done during the experiment. However, the measurement of pH at the end of the experiments indicated that this parameter had been kept constant within a ± 0.2 pH units.

The effect of increasing the hydrogen overpressure in the system on the measured uranium concentrations in solution can be seen in Figure 14.

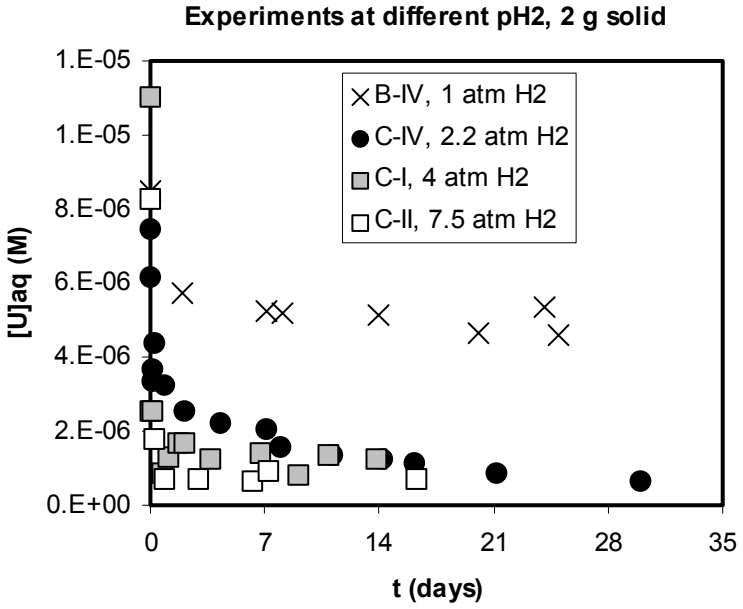

Figure 14. *Evolution of the aqueous uranium concentration with time. Effect of the $H_2(g)$ overpressure.*

We can see that the increase in the hydrogen pressure in the system causes a faster decrease in the uranium concentrations in solution and also that lower final uranium concentrations are obtained.

The effect of an increase in the mass of solid in contact with the solution at a fixed $H_2(g)$ pressure can be observed in Figure 15. From this plot we can see that when increasing the mass of solid the decrease in the concentrations of uranium in solution seems to be faster. However, when using a large amount of magnetite, 5 g, the decrease is not as fast as expected. This could be caused by a precarious contact between the solid and the solution, given the difficulty associated to the stirring of the experiments conducted in the autoclave.

As in the case of the experiments conducted at a total pressure of 1 atm, we have superimposed the final concentrations measured in solution to a solubility curve of the solid most likely to be precipitating in the system, $UO_2(am)$. The results can be seen in Figure 16, where the experimental range of uranium concentrations measured in the experiments is shown with a shadowed area, what indicates that the system is behaving as being buffered in the pe range from –3 to –2, in agreement with the results in Figure 13 for the experiments conducted at 1 atm $H_2(g)$.

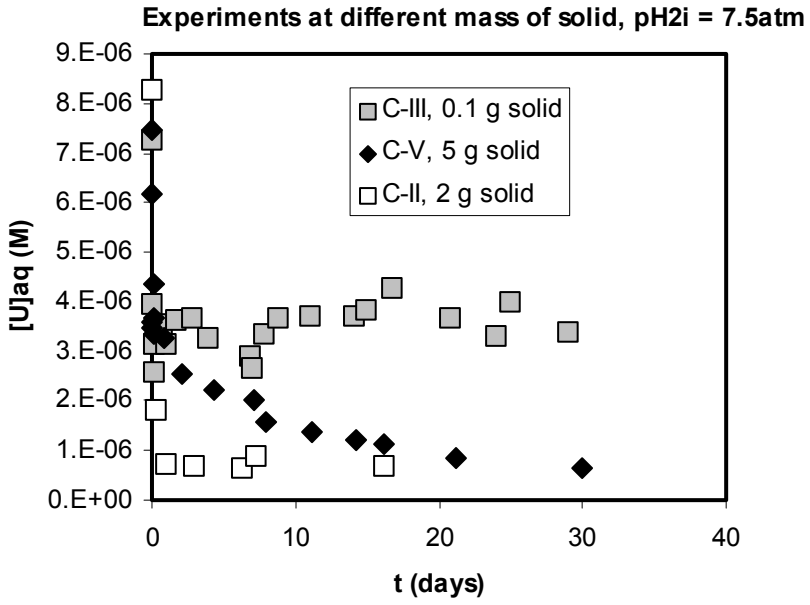

Figure 15. *Evolution of the aqueous uranium concentration with time. Effect of the mass of solid. Experiments conducted at an intial $pH_2(g)$ in the range 7–8 atm.*

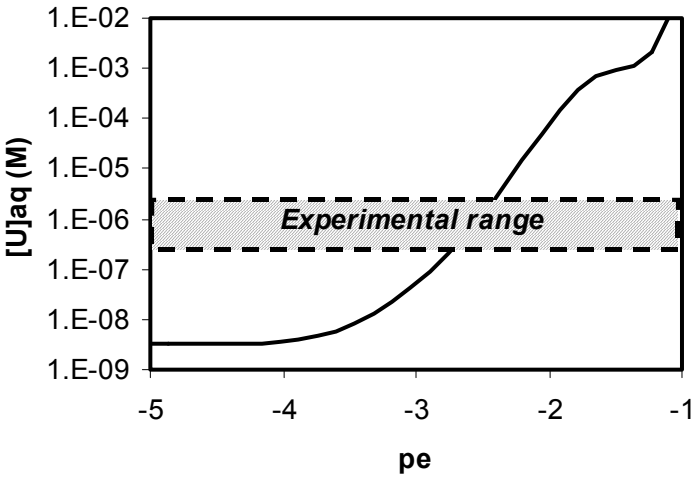

Figure 16. *Range of experimental uranium concentrations measured in the system in comparison with the solubility of UO_2(am). The solubility curve has been calculated at pH = 8.3, the one measured in the experiments.*

After the experiment performed at 7.5 atm and 5 g of magnetite, the uranium onto the magnetite solid surface was analysed by using XPS. In spite of the low uranium concentration in the solid, the characteristic uranium $4f_{7/2}$ peak was recorded. The treatment of this peak showed a shift from 382.0 eV (characteristic of U(VI)) to 381.4 eV, indicating a reduction of the uranium (VI) probably mediated by the magnetite surface (see Figure 17).

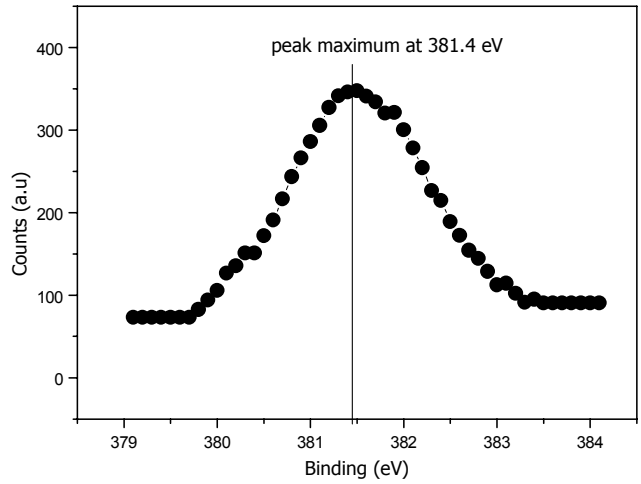

Figure 17. *Uranium $4f_{7/2}$ peak showing the peak maximum at 318.4 eV.*

3.5 Effect of in-situ generated magnetite on the behaviour of U(VI) at $pH_2(g)$ = 1 atm

Generation of magnetite via steel corrosion

The chemical composition of the fresh coupons used in the experiments, determined by EDS (Energy Dispersive Spectrometer) semi-quantitative analysis, was found to be approximately: Fe 97 wt% and C 3% wt%.

After appropriate exposure to a corrosive environment of carbon steel coupons (see Experimental section, 2.3.c), the specimens were removed from the autoclave reactor. Due to this procedure the colour of the coupons changed to black and no significant weight losses were detected due to corrosion.

The nature of the corrosion products formed on the coupons surface was investigated through XRD (X-Ray Diffraction). A representative XRD pattern obtained from the surface of the coupon is presented in Figure 18 which shows the presence of magnetite.

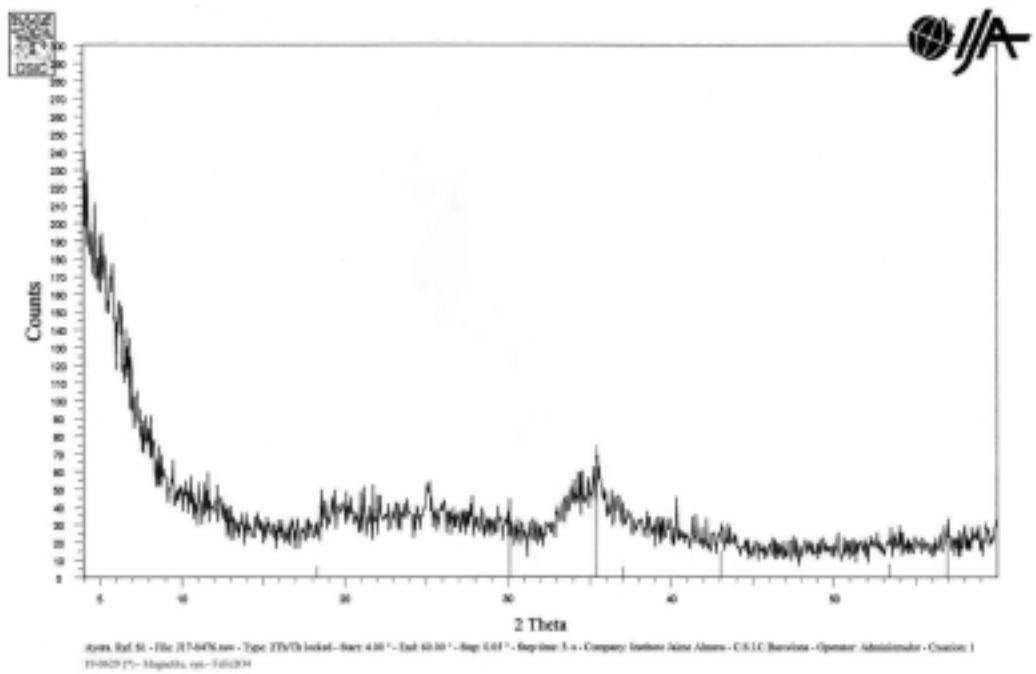

Figure 18. *XRD pattern from a coupon exposed to a anaerobic $NaHCO_3$/NaCl medium for 54 day. (T = 90ºC and $P(H_2)$ = 8.4 atm).*

Interaction U(VI)-steel (Test D-I)

Two different tests were performed on the interaction of U(VI) with the product of the corrosion of the steel coupon: D-I, corresponding to the first stage of the project at 1 atm $H_2(g)$ and D-II, in which a constant $pH_2(g) + pCO_2(g) = 1$ atm with $pCO_2(g) = 10^{-3.8}$ was kept through the system. An additional experiment conducted in a similar way to experiment D-II but by using the fresh steel coupon was set up in order to see the influence of the corrosion on the U(VI) system. The experimental conditions are presented in Table 6.

Table 6. Experimental conditions of the tests conducted with the steel coupon.

Test		[U]o (M)	Ctot or pCO_2	$PH_2(g)$ $+pCO_2(g)$
D-I	Corroded Coupon	$8.1 \cdot 10^{-6}$	$5 \cdot 10^{-4}$	1
D-II	Corroded Coupon	$8.1 \cdot 10^{-6}$	–3.82*	1
FE	Fresh Coupon	$8.1 \cdot 10^{-6}$	–3.82*	1

* log $pCO_2(g)$ kept constant

The evolution of the uranium concentration in solution with time are shown in Figure 19.

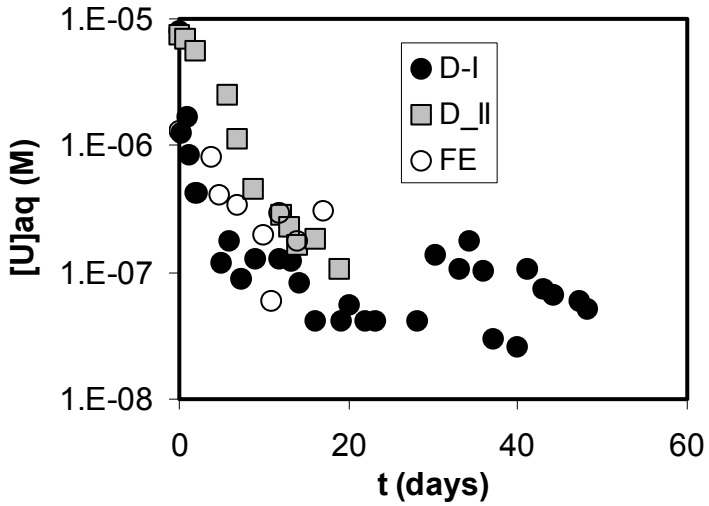

Figure 19. *Evolution of the aqueous uranium concentration with time in the experiments conducted with the corroded coupon (D-I and D-II) and with the fresh steel coupon (FE).*

In spite of the fact that in experiments D-II and FE no steady-state has been yet attained, what we can see from this figure is that the concentration of uranium decreases to lower levels than in the case of using magnetite. This can be due to the fact that the presence of iron from the steel produces a decrease in the redox potential of the system and, therefore, the reduction process is more effective. Given that this is also observed with the fresh steel surface, the fact that a sorption process accounts for the decrease of the uranium concentration in solution does not seem to be a valid explanation because of the lower effective surface area of the polished surface of the clean coupon in comparison with magnetite and the corroded surface.

The presence of zerovalent iron in experiment D below the magnetite surface might account for an increase of the electronic density at the surface and, therefore, might facilitate the electronic transference, causing a preferential oxidation of the structural iron in front of the experiment conducted in the absence of steel. Furthermore, the formation of amorphous iron phases as corrosion products of steel may help to the reduction process given that the ability to sorb uranium is increased with the surface area of the solid.

The ability of metallic iron to reduce uranium(VI) under anoxic conditions has been a matter of study by several authors /Fiedor et al, 1998; Gu et al, 1998/ due to the feasibility of installing reactive barriers to remediate uranium contaminated groundwaters. The results indicate that Fe^0 is very efficient in reductively precipitate uranium(VI) from solution, not only under reducing but also under anoxic conditions. This would indicate that the actual reductant in the system is not hydrogen, but magnetite, ferrous iron provided by its dissolution, or iron in the case of having steel in the system.

The comparison between the final U concentration achieved in the system and the solubility of UO_2(am) is shown in Figure 20.

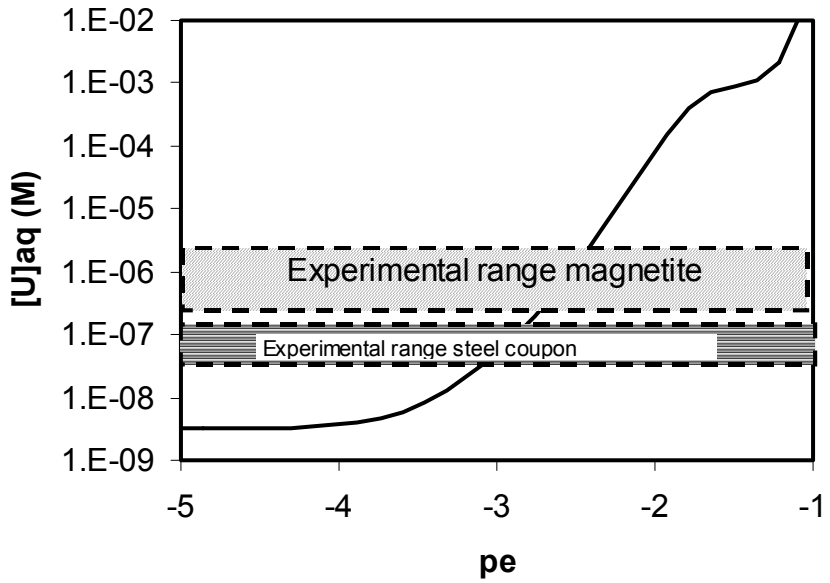

Figure 20. *Solubility of UO_2(am) as a function of pe. The shadowed areas correspond to the range of uranium concentrations measured in the experiments conducted by using magnetite and corroded or fresh steel coupons.*

Spectroscopic characterisation

During the time span (several days) comprised between the extraction of the coupon from the autoclave and the beginning of test D-I, a change in the coupon colour, black to green, was observed likely caused by the coupon with air (see Figure 21). The green colour might be attributed to the presence of carbonate green rust GR(CO_3). Green rusts are unstable Fe(II)-Fe(III) hydroxy-salts which constitute transient compounds between metallic iron and final corrosion products and therefore may govern the mechanisms and kinetics of corrosion and passivation of iron-based alloys in aqueous media. Due to their instability, their identification as corrosion products of iron and steel is rarely reported /Refait et al, 1998/. /Savoye et al, 2001/, reported that the conditions that seem to be in favour to the formation of carbonate green rust are: low $NaHCO_3$ concentration and low residual O_2 content at 90ºC, which coincide with the conditions employed during the corrosion procedure used in this work.

After the completion of experiment D-I, we have performed a spectroscopic characterization of the corroded coupon contacted with the uranium solution. The specimen surface was investigated by XRD and SEM (Scanning Electron Microscopy) equipped with EDS.

Figures 22 and 23 shows SEM examinations of the fresh specimen surface and the coupon surface after the corrosive treatment and exposure to an uranium solution during Test D-I. It can be observed the surface alteration due to corrosion, compared to the untreated carbon steel. In order to identify the main chemical elements at the coupon surface, EDS mappings of several elements were performed. Figures 24, 25 and 26, show iron, oxygen and uranium mapping results respectively corresponding to the same coupon zone presented in Figure 23.

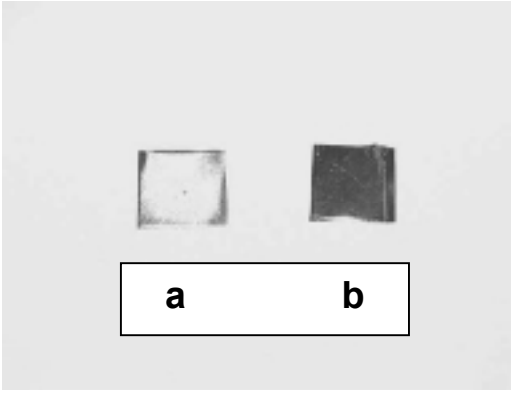

Figure 21. *Carbon steel coupons: a) fresh and b) corroded and exposed to air.*

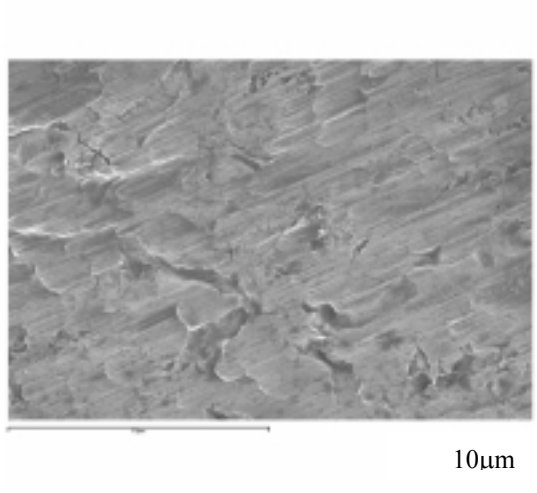

Figure 22. *SEM image of the fresh coupon.*

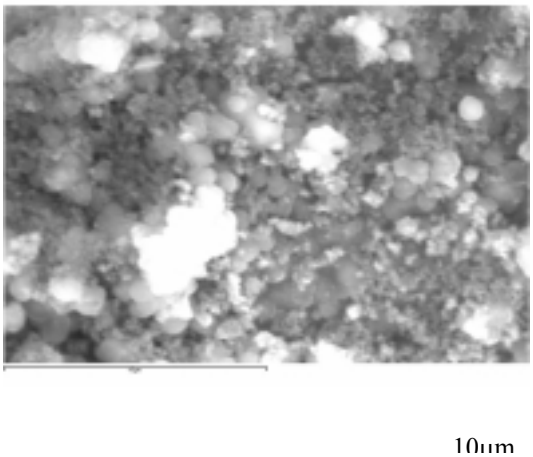

Figure 23. *SEM image of the corroded coupon after the experiment D-I.*

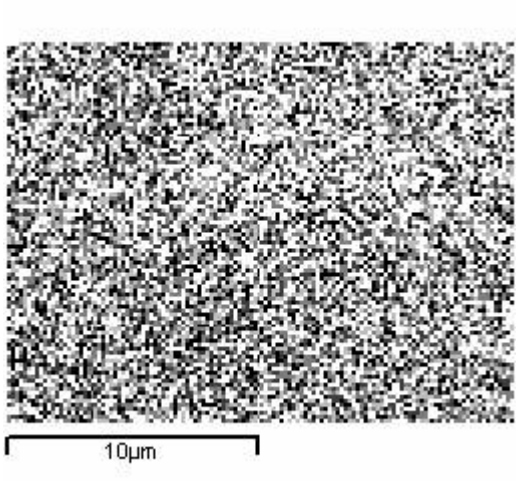

Figure 24. *Iron mapping (EDS) corresponding to the image presented in Figure 23.*

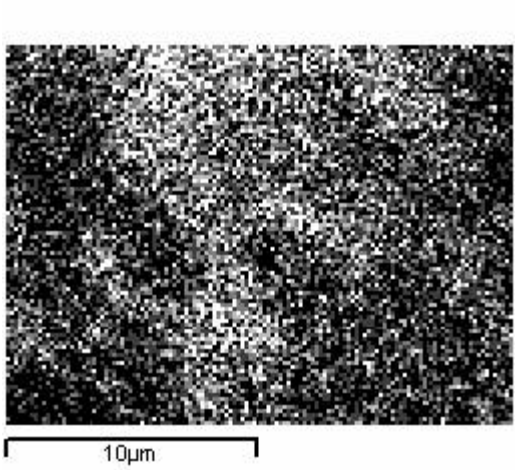

Figure 25. *Oxygen mapping (EDS) corresponding to the image presented in Figure 23.*

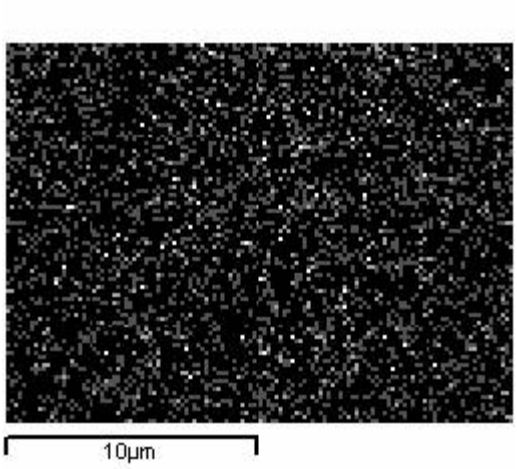

Figure 26. *Uranium mapping (EDS) corresponding to the image presented in Figure 23.*

It can be seen a uniform distribution of oxygen, iron and uranium on the coupon surface. Other elements identified were, potassium and silicon, impurities probably arising from the glass vessel used in the corrosion process. The EDS semi-quantitative analyses, which are sensitive up to a depth of several microns, allowed to determine an uranium content in the area investigated of 2.5 wt%.

XRD analysis evidenced the presence of magnetite and lepidocrocite on the coupon surface. Green rust and uranium crystalline phases were not identified on the coupon. In fact, the theoretical uranium concentration on the bulk coupon calculated through a mass balance using data obtained in test D-I is very low: 0.02 wt%. If we consider the two sides of the coupons assuming an active thickness of 5 μm each one (total coupon thickness: 1mm), then the estimated uranium concentration at the surface becomes 2 wt%, which was not high enough to be detected by XRD. However this value is in good agreement with the previous estimation of an active thickness of the coupon sides of 5 μm.

In order to clean the coupon surface surface and remove uncoated particles and impurities no related to the adsorption/precipitation processes, the coupon was contacted during 15 minutes with ketone in an ultrasonic bath. After this treatment, SEM images and the EDS spectra obtained did not suffer any remarkable variation in comparison with the previous results obtained, confirming the strong interaction between uranium as well as the impurities detected with the carbon steel coupon.

3.6 Kinetics of the reduction process

The kinetics of the reduction process may depend on different factors. Previous works have reported that the hydrogen pressure influences to a large extent the rate of the process /Forward and Halpern, 1953/. These authors also found a direct relationship between the rate of reduction and the concentration of cataliser, i.e. the surface area available for coordination.

From our results we have observed a similar trend, i.e,. a direct influence of the hydrogen pressure. However we have not seen any influence of the surface area on the rate of the process in the range of surface areas we have worked with.

Influence of the H_2(g) pressure

First of all we can compare the results obtained at 1 atm total pressure of N_2(g) in front of 1 atm of H_2(g) (see Figure 27).

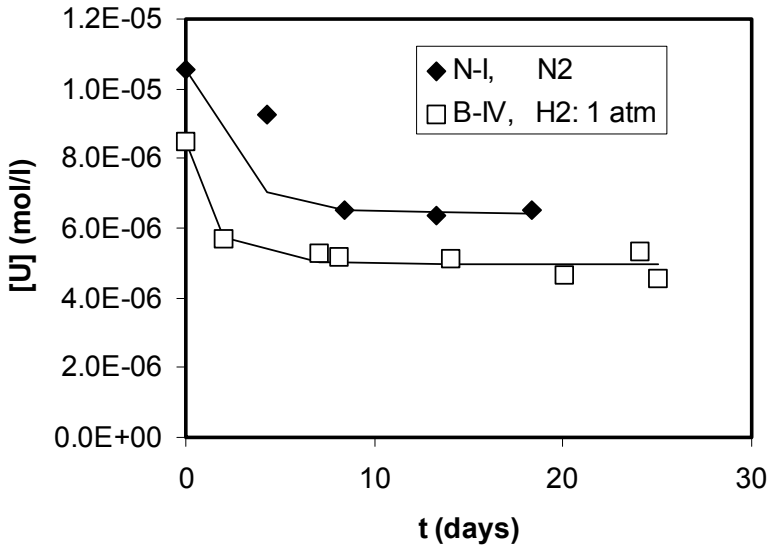

***Figure 27**. Influence of H_2(g) or N_2(g) pressure on the rate of decrease of the concentration of uranium in solution in contact with commercial magnetite.*

From this figure we can see that the final concentration of uranium in the system is lower in the case of working with hydrogen than when using nitrogen.

The effect of increasing the concentration of hydrogen in the experiments is to accelerate the rate of reduction of uranium, as it can be seen from Figure 28.

In order to quantify the effect of an overpressure of hydrogen on the rate of uranium reduction we have assumed that the process occurring in the system can be depicted by the following equation:

$(UO_2)_2CO_3(OH)_3^- + 5\ H^+ + 4\ e^- = 2\ UO_2(s) + CO_2(g) + 4\ H_2O;$

with a direct rate of k_1 and an inverse k_{-1} rate of reaction.

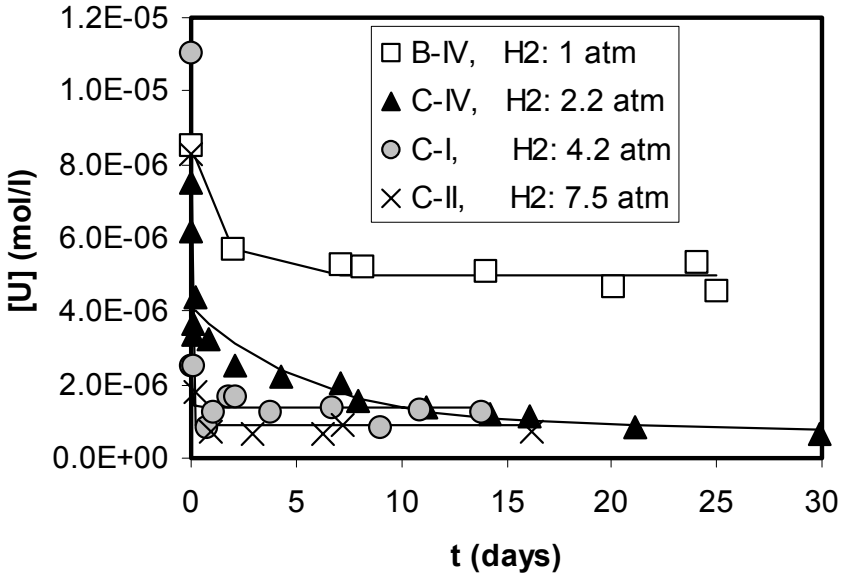

Figure 28. *Influence of $H_2(g)$ pressure on the rate of decrease of the concentration of uranium in solution in contact with commercial magnetite.*

According to the previous reaction we can say that the rate of uranium reduction in the system can be given by the following equation:

$$\frac{dU}{dt} = -2k_1.\left[(UO_2)_2CO_3(OH)_3^-\right] + k_{-1}$$

Solving this equation between $U(t=to) = Uo$ and $U(t=t) = Ut$, we arrive to the following expression:

$U = A + B\ exp(-k_1 t)$

where $A = U_o - \frac{k_{-1}}{k_1}$ and $B = Uo - A$.

By adjusting the former equation to the experimental data we have obtained the different parameters: A and B, therefore k_1, k_{-1} and Uo, that we compare in Table 7.

Table 7. Parameters resulting from the adjustment of Equation (3) to experimental data at different pH2(g).

$p(H_2)$	**0**	**1**	**2.2**	**4**	**7.5**
Exp.	**N-I**	**B-IV**	**C-IV**	**C-I**	**C-II**
A	$(5.77\pm1.39)\cdot10^{-6}$	$(4.99\pm0.13)\cdot10^{-6}$	$(7.9\pm2.8)\cdot10^{-7}$	$(1.36\pm0.15)\cdot10^{-6}$	$(9\pm2)\cdot10^{-7}$
B	$(4.98\pm1.45)\cdot10^{-6}$	$(3.49\pm0.44)\cdot10^{-6}$	$(3.32\pm0.45)\cdot10^{-6}$	$(9.65\pm0.50)\cdot10^{-6}$	$(7.4\pm0.5)\cdot10^{-6}$
k_1	0.14±0.10	0.78±0.26	0.17±0.06	50.±10	69.5
Uo	$1.08\cdot10^{-5}$	$8.48\cdot10^{-6}$	$4.11\cdot10^{-6}$	$1.10\cdot10^{-5}$	$8.29\cdot10^{-6}$
Uo real	$1.05\cdot10^{-5}$	$6.50\cdot10^{-6}$	$7.48\cdot10^{-6}$	$1.10\cdot10^{-5}$	$8.27\cdot10^{-6}$
Ueq	$5.77\cdot10^{-6}$	$4.99\cdot10^{-6}$	$7.87\cdot10^{-7}$	$1.39\cdot10^{-6}$	$9.00\cdot10^{-7}$

What we observe from the previous results is that the value of k_1, i.e. the rate at which the concentration of uranium in solution decreases, increases with $pH_2(g)$. In Figure 29 we have plotted the value of k_1 versus $pH_2(g)$ and we see a linear relationship between both parameters.

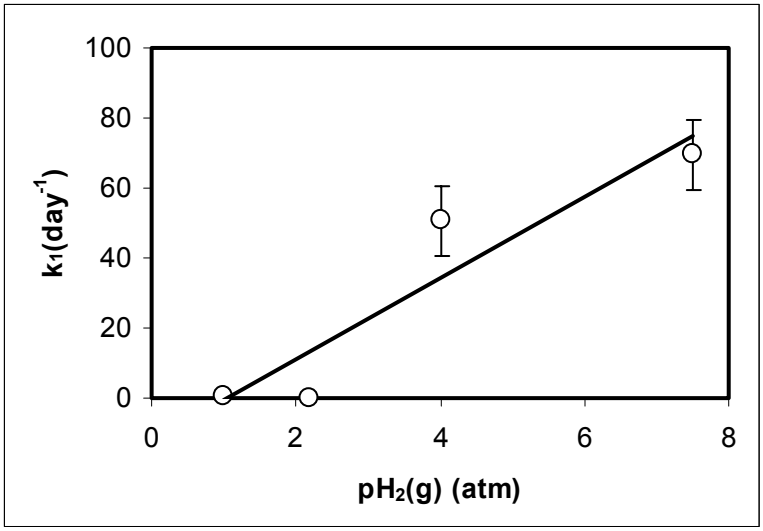

Figure 29. *Influence of the H_2 overpressure on the kinetic constant k_1.*

The linear regression of the data produces a slope of 11.6±3.2 $day^{-1} \cdot atm^{-1}$, with a correlation coefficient of 0.87.

/Bunji and Zogovic, 1958/ studied the effect of UO_2(s) on the U(VI) reduction process working at H_2 overpressures in the range 10 to 20 atm. By conducting the same adjustment to their data (Figures 30 and 31) a slope of 0.48 day^{-1} atm^{-1} has been obtained. We also see from these author's data that k_1 values obtained are lower than the ones we have obtained with magnetite, what can be an indication of the ability of the cataliser in favouring the reduction reaction.

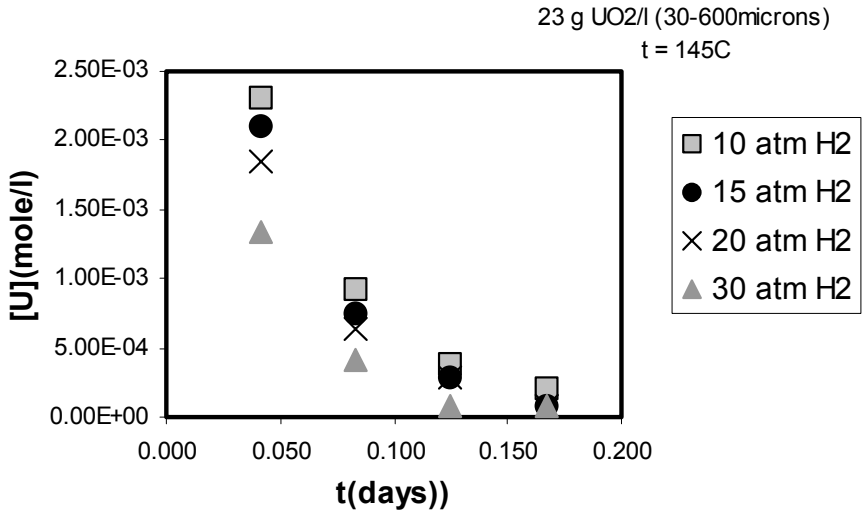

Figure 30*. Influence of the pressure hydrogen on the rate of decrease of the concentration of uranium in solution (Data from /Bunji and Zogovic, 1958/).*

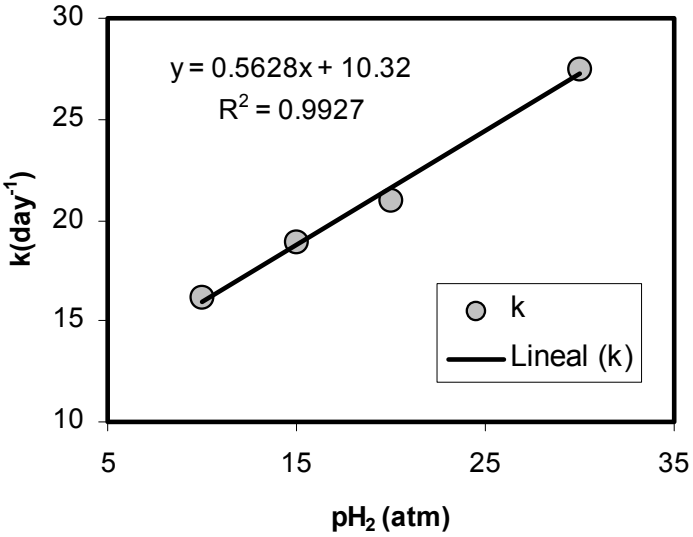

Figure 31. *Influence of the H_2 overpressure on the kinetic constant k_1 (Data from /Bunji and Zogovic, 1958/).*

Influence of the mass of solid

We conducted three different experiments conducted at initial H_2 overpressures between 7.5 and 8.6 atm (C-II, C-III and C-V in Table 1) at different solid to liquid ratio. No clear influence of the mass of solid is observed, (see Figure 32) what can be due to a not sufficiently vigorous stirring in the experiments. This can be seen in the case of the experiment conducted with 5 g of magnetite, where after a fast initial decrease of the concentration of uranium there is a somewhat slower decrease that can be attributed to diffusion processes of the solution in the bulk of the solid. This does not happen with the experiment conducted with the lowest amount of magnetite given that the solid to solution contact is much more effective.

A priori we would expect an increase in the rate of reduction of uranium with the amount of surface available given that we are assuming that its reduction is a surface mediated process and in agreement with other authors /Forward and Halpern, 1953/.

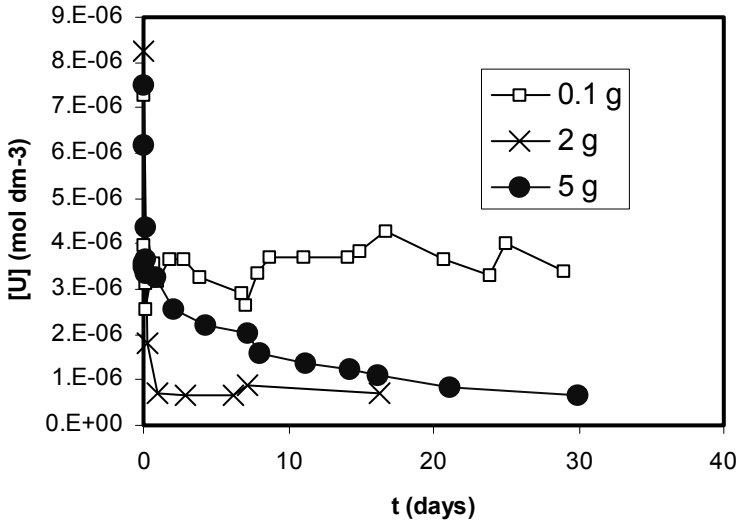

Figure 32. *Effect of the mass of solid to liquid ratio on the rate of decrease of the concentration of uranium in solution*.

3.7 XAS analyses

The aim of this experiment is to examine the structure and the oxidation state of uranium sorbed onto the surface of magnetite (Fe_3O_4) and FeO-rich olivine. The U L3-edge XANES spectra can be useful to derive information about the oxidation state of actinides on the solid surface /Morris et al, 1996; Conradson et al, 1998/.

Four different uranium standards were analysed: U(VI): $UO_3 \cdot 2H_2O$; U(IV) UO_2(s); U(VI) and U(IV): U_3O_8(s) and 50% $UO_3 \cdot 2H_2O$ + 50% of UO_2(s). Sorption of U(VI) onto the magnetite and the olivine samples was conducted at 25ºC from a homogeneous solution containing 10^{-5} mole/dm^3 of U(VI) at pH ranging from 6 to 7 and by continuous N_2 or H_2 (g) bubbling. XAS spectra of the samples were recorded by fluorescence detection, due to the low uranium content. We have proceeded in a manner similar to that of Conradson et al, 1998 and Morris et al, 1996 to de-convolute all the signals obtained for our samples and we have obtained a "calibration curve" (see Figure 33) of the oxidation state of uranium by using the data from our standards. We have then obtained the theoretical ratio U(VI) to U(IV) in the uranium-coated olivine and magnetite samples.

Figure 33a shows a typical XANES spectrum of our samples with the deconvolution of the signal in the different components previously mentioned. The resulting shifts of the standards and the samples analysed are presented in Figure 33b. The parameters of the calibration curve are the following:

%U(VI) = (12.459±0.869)·(SHIFT) – (124.37±12.465); with r^2 = 0.9808.

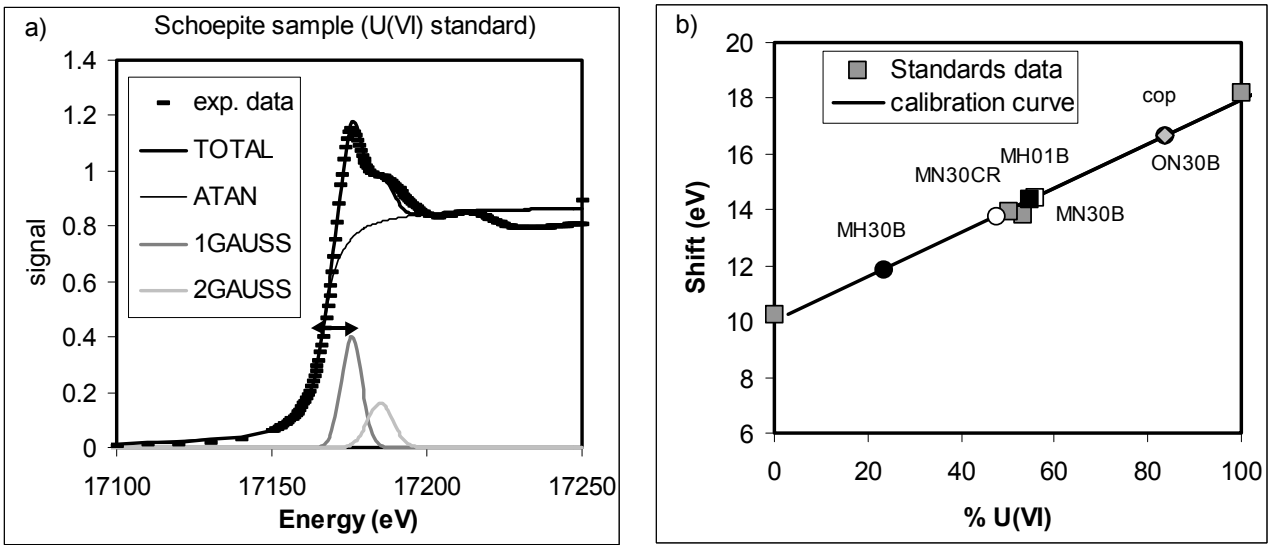

Figure 33. *a) XANES spectrum of the U(VI) standard and de-convolution of the peak into an ATAN and two Gaussian functions. The arrow indicates the shift used for the determination of the U(VI) to U(IV) ratio in the sample. b) Calibration curve of the shift over the percentage of U(VI) in the samples obtained by using data on the standards and data of the samples superimposed. M: magnetite; O: olivine; H and N indicates preparation under hydrogen (reducing) or nitrogen (anoxic) conditions; 01 and 30: days of contact between solid and U(VI) solution; "cop" sample prepared by coprecipitation of U(VI) with Fe(III), no U(VI) reduction to U(IV) is possible.*

Sample MH30B, that was prepared under more reducing conditions and for which the interaction magnetite-Uranium was allowed to proceed for the longest time (30 days), plots at the lowest %U(VI), indicating that reduction of uranium has proceeded. Sample prepared with U(VI) and Fe(III) for which no reduction is feasible, plots in the highest range of the graph. There is some error in this analyses, given that this sample should plot on the right axis (U(VI) = 100%) and it behaves as if it had only a 83.5% of U(VI). This deviation can be also due to the different coordination environment of the samples, that is, the fact that the substrate in this case was ferrihydrite while in the other cases were either olivine, magnetite or uranium pure phases for the standards. In general, this analyses permits a rather good estimation of the percentage of reduction of U(VI) to U(IV).

What can be concluded from these analyses is that there is an effective reduction of the uranium(VI) initially in contact with magnetite to U(IV). This technique has been very useful to complement data obtained from aqueous chemistry and see that the reduction process is active in the system.

4 Conclusions

- From preliminary experiments, it has been concluded that both redox electrodes, platinum and gold, have a response that seems to be related to the ratio oxidizing/reducing species in solution (uranium and iron) of the redox pairs involved in the system.

- In the experiments performed contacting commercial magnetite with U(VI) under H_2 atmosphere (1 atm), the measured uranium concentrations agree with the solubility of UO_2(am) at the experimental conditions employed, and therefore that we may assume that a reduction process is occurring in the system.

- Concerning the results obtained in tests performed at $P(H_2) > 1$ atm using an autoclave reactor, it was observed that the increase in the hydrogen pressure in the system causes a faster decrease in the uranium concentrations in solution. Also, the experimental range of uranium concentrations measured in the experiments is in well agreement with UO_2(am) solubility, assuming that pe values (which were not measured in the autoclave) are in the range of those measured in experiments at 1 atm H_2(g). XPS results indicate the reduction of U(VI) onto the magnetite solid surface.

- In the range of magnetite surface areas we have performed the experiments, no influence of the surface area on the process rate has been observed. However, a bad contact between the solid and the solution can be the reason of this finding.

- Taking into account the experimental results obtained working with in-situ generated magnetite on the behaviour of U(VI), it seems that the presence of zerovalent iron below the magnetite surface might account for an increase of the electronic density at the surface and, therefore causing a preferential oxidation of the structural iron in front of the experiment conducted with commercial magnetite. Furthermore, the formation of amorphous iron phases as corrosion products of steel may help to the reduction process given that the ability to sorb uranium is increased with the surface area of the solid. Uranium concentration seems also to be controlled by UO_2(am) solubility.

- From XAS analyses of magnetite samples previously contacted with U(VI), data obtained from aqueous chemistry has been complemented, and it has been observed that there is an effective reduction of the uranium(VI) initially present in the system.

5 Acknowledgements

This work has been financially supported by SKB. The authors wish to thank the Rossendorf Operating Beam Line of the European Research Synchrotron Facility for the possibility and financial support to conduct the XANES measurements of the magnetite samples and Montse Marsal from UPC for SEM examinations

6 References

Blackwood D J, Naish C C, Platts N, Taylor K J, Thomas M I, 1995. The anaerobic corrosion of carbon steel in granitic groundwaters. SKB Report 95-03. Svensk Kärnbränslehantering AB.

Bunji B, Zogovic B, 1958. Reduction of uranium from carbonate solutions with hydrogen using UO2 as catalyst. In Proceedings of the International Conference on the Peaceful Uses of Atomic Energy, Geneva, P/485, 350–355.

Conradson S D, Al Mahamid I, Clark D L, Hess N J, Hudson E A, Neu M P, Palmer P D, Runde W H, Tait C D, 1998. Polyhedron, Vol 17, No 4, pp 599–602.

El Aamrani F, Casas I, de Pablo J, Duro L, Grivé M, Bruno J, 1999. Experimental and modelling study of the interaction between uranium(VI) and magnetite. SKB TR-99-21. Svensk Kärnbränslehantering AB.

Fiedor J N, Bostick W D, Jarabaek R J, Farrell J, 1998. Understanding the mechanism of uranium removal from groundwater by Zero-Valent iron using X-Ray photoelectron spectroscopy. Env. Sci. Technol., 32, 1466–1473.

Forward F A, Halpern J, 1953. Precipitation of uranium from carbonate solutions by reduction with hydrogen. Trans. Can. Inst. Mining Mat., 56, 645–648.

Gibbs C, 1976. Characterization application of ferrozine iron reagent as ferrous iron indicator. Anal. Chem., Vol 48, 8, 1197–1200.

Gu B, Liang L, Dickey M J, Yin X, Dai S, 1998. Reductive Precipitation of Uranium(VI) by Zero-Valent Iron. Env. Sci. Technol., 32, 3366–3373.

McIntyre M R, Zetaruk D G, 1977. X-Ray photoelectron spectroscopy studies of iron oxides. Anal. Chem. 49, 1521–1529.

Morris D E, Allen P G, Berg J M, Chisholm-Brause C J, Conradson S D, Donohoe R J, Hess N J, Musgrave J A, Tait C D, 1996. Environ. Sci. Technol., 30, 2322–2331.

Neck V, Kim J I, 2001. Solubility and hydrolysis of tetravalent actinides. Radiochim. Acta 89, 1–16.

Parkhurst D L, Appelo C A J, 1999. User's Guide to PHREEQC (version 2) – A Computer Program for Speciation, Batch-Reaction, One-Dimensional Transport, and In-verse Geochemical Calculations. USGS Water-Resources Investigations Report 99-4259.

Refait P H, Abdelmoula M, Génin J-M R, 1998. Mechanisms of formation and structure of green rust one in aqueous corrosion of iron in the presence of chloride ions. Corrosion Science 40, 1547–1560

Savoye S, Legrand L, Sagon G, Lecomte S, Chausse A, Messina R, Toulhoat P, 2001. Experimental investigations on iron corrosion products formed in bicarbonate/ carbonate-containig solutions at 90ºC. Corrosion Science 43, 2049–2064

White A F, Peterson M L, Hochella M F, 1994. Electrochemistry and dissolution kinetics of magnetite and ilmenite. Geochim. et Cosmochim. Acta 58(8) 1859–1876.

White A F, Peterson M L, 1996. Reduction of aqueous transition metal species on the surfaces of Fe(II) containing oxides. Geochim. et Cosmochim. Acta 60(20) 3799–3814.

ISSN 1404-0344

CM Digitaltryck AB, Bromma, 2003